Lab Notes

Editors
Thomas M. Moses | Shane F. McClure

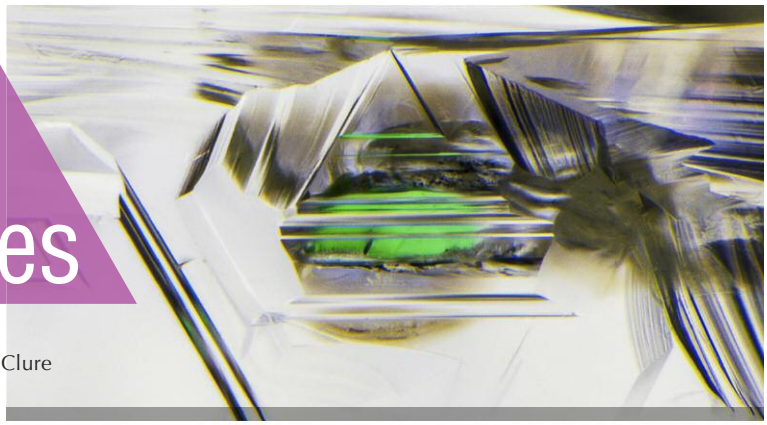

Faceted CHIOLITE

Recently, the GIA lab in Carlsbad received a colorless 1.04 ct gemstone of a material that was new to the lab (figure 1). The measured refractive index was 1.342–1.349 with a birefringence of 0.007 and an optic character of uniaxial negative. The specific gravity, measured hydrostatically, was 3.01. These properties were consistent with the mineral chiolite, which was confirmed by Raman spectroscopy (see figure 2 and http://rruff.info/R050412).

Chiolite is a very rare transparent to translucent colorless or snow-white mineral with a vitreous luster, perfect cleavage in one direction, and a white streak. It crystallizes in the tetragonal system and is composed of sodium and aluminum, with the formula $Na_5Al_3F_{14}$ (the presence of these elements was confirmed with EDXRF). The principal source of gem-quality material is Ivigtut, Greenland, where it occurs in association with cryolite. Other gem-quality sources include Miass in the Ilmen Mountains region of Russia, where it is found in a cryolite pegmatite, and the Morefield pegmatite mine in Virginia (see AZoMining.com). The mineral was first discovered at Miass in 1846. The name is very similar to cryolite, a related mineral. *Cryolite* comes from Greek for "ice stone," while *chiolite* means "snow stone." Like their namesakes, they are sometimes found together, though chiolites are rarer.

Figure 1. This 1.04 ct colorless octagonal cut was identified as chiolite.

This gem has a very low hardness (3.5–4 on the Mohs scale) and perfect cleavage. The stones are usually small and nondescript. Nevertheless, chiolite has joined the ranks of minerals cut by faceters who wish to try their hand at everything clean enough to cut, and a cut stone would make quite a specimen for a gem collection.

Chiolite occurs in some granite pegmatites and is associated with ralstonite, pachnolite, elpasolite, cryolite, thomsenolite, cryolithionite, fluorite, phenakite, and topaz (see mindat.org and rruff.info).

Figure 2. Raman spectroscopy confirmed the colorless stone's identity as chiolite.

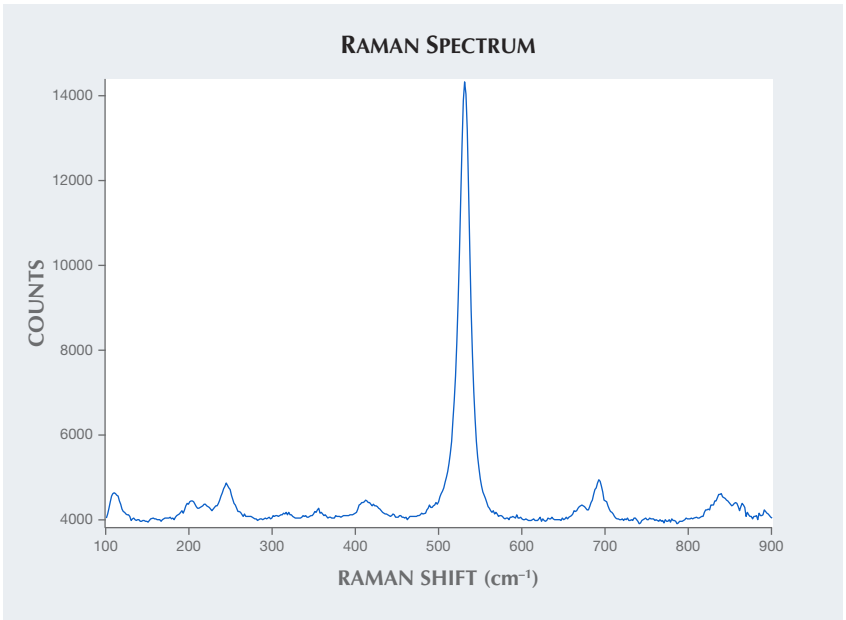

Editors' note: All items were written by staff members of GIA laboratories.

Gems & Gemology, Vol. 55, No. 3, pp. 416–425.

© 2019 Gemological Institute of America

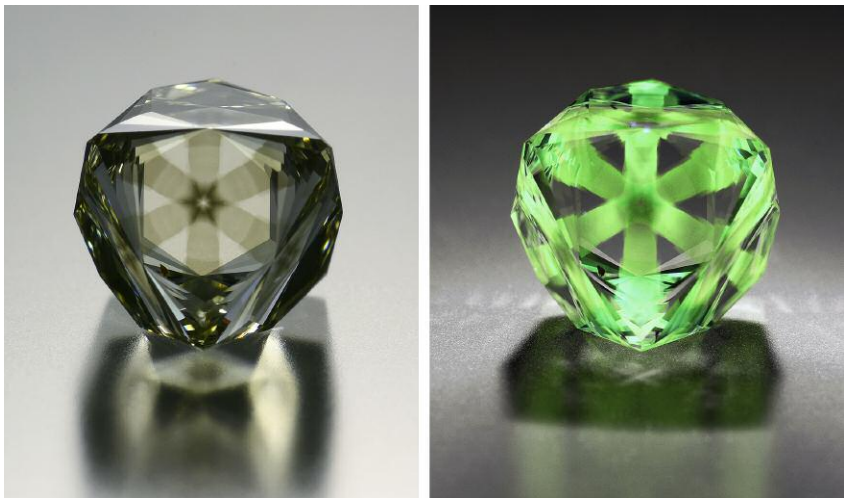

Figure 3. This 3.70 ct brownish greenish yellow faceted octahedron contained a remarkable stellate hydrogen cloud (left) that showed strong yellowish green fluorescence under long-wave UV light (right).

Chiolite is difficult to cut, extremely rare, and has little commercial appeal. It is solely a curiosity in the gem world.

Forozan Zandi

Faceted DIAMOND Octahedron with a Remarkable Stellate Cloud Inclusion

A 3.70 ct faceted Fancy brownish greenish yellow diamond (figure 3, left) was recently submitted to the Carlsbad laboratory for color origin and identification service. The diamond was remarkable in that it contained an eye-visible stellate cloud inclusion consisting of six legs that each radiated to a point on the polished octahedron. Diamonds containing star-like clouds are sometimes referred to as "asteriated" in the trade (T. Hainschwang et al., "The Rhodesian Star: An exceptional asteriated diamond," *Journal of Gemmology*, Vol. 34, No. 4, 2014, pp. 306–315). While GIA occasionally encounters asteriated diamonds, this one was striking due to the well-defined nature of the star and the strong yellowish green color it exhibited under long-wave UV (figure 3, right).

Gemological examination revealed a type Ia diamond, showing a typical cape series in the visible spectrum. Hydrogen bands in the infrared spectrum and the UV-Vis-NIR spectrum were consistent with the observed "hydrogen cloud" inclusions (figure 4). These clouds in diamonds consist of a high density of light scattering micro-inclusions consistent with those that have been reported to be graphite (B. Rondeau et al., "Three historical 'asteriated' hydrogen-rich diamonds: Growth history and sector-dependent impurity incorporation," *Diamond and Related Materials*, Vol. 13, No. 9, 2004, pp. 1658–1673) that correlate strongly with the presence of hydrogen (W. Wang and W. Mayerson, "Symmetrical clouds in diamond—the hydrogen connection," *Journal of Gemmology*, Vol. 28, No. 3, 2002, pp. 143–152). Also observed was brown radiation staining in a shallow feather, indicating that the stone had been exposed to natural alpha radiation (figure 5).

While the cutting style was unconventional, it served to showcase the remarkable inclusion scene contained within the diamond. This is one of the most interesting diamonds of this type examined at GIA's Carlsbad laboratory.

Maryam Mastery Salimi and Nathan Renfro

Figure 4. The six-ray star pattern is composed of microscopic particles commonly referred to as "hydrogen clouds" (left) that fluoresce strong green to long-wave UV (right). Field of view 6.27 mm.

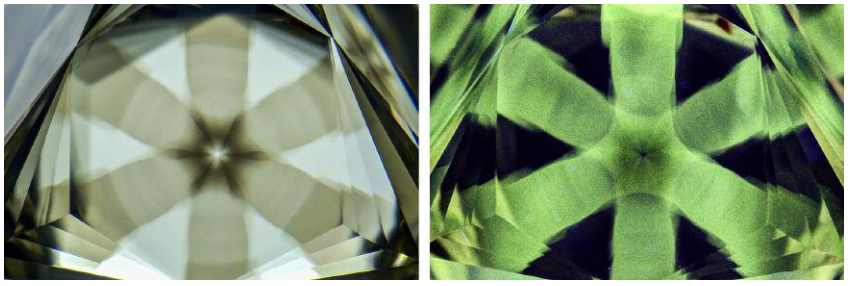

GROSSULAR GARNET Crystals in Demantoid Garnet

Demantoid, the green variety of andradite garnet, is a rare gemstone. It typically possesses high dispersion and diamond-like luster, which is often partly masked by the green and yellow-green bodycolors. Variations

Figure 5. An irregularly shaped dark brown radiation stain on the diamond's surface-reaching inclusion clearly shows that it was exposed to natural alpha radiation. Field of view 3.51 mm.

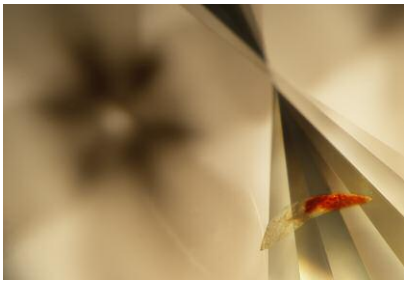

TABLE 1. LA-ICP-MS results on three areas of the demantoid sample: the host material (spot 1), the outer area of the inclusion (spot 2), and the inner area of the inclusion (spot 3).

Concentration (ppmw) of different elements	Mg	Al	Si	Ca	Ti	V	Cr	Mn	Fe	
Spot 1	449	414	185000	275000	17.7	nd[a]	nd	328	186000	
Spot 2	162	32200	205000	296000	338	4.66	nd	723	152000	
Spot 3	127	85100	192000	271000	3570	10.4	nd	13000	57600	
Detection limits (ppmw)	0.17	0.92	221	36	0.65	0.06	0.80	0.15	5.03	
Wt.% oxides, converted from LA-ICP-MS	**MgO**	**Al_2O_3**	**SiO_2**	**CaO**	**TiO_2**	**V_2O_5**	**Cr_2O_3**	**MnO**	**FeO**	
Spot 1	0.1	0.1	39.6	38.5	0.0	nd	nd	0.0	23.9	
Spot 2	0.0	6.1	43.9	41.4	0.1	0.0	nd	0.1	19.6	
Spot 3	0.0	16.1	41.1	37.9	0.6	0.0	nd	1.7	7.4	
Normalized to 12 oxygen atoms	**Mg**	**Al**	**Si**	**Ca**	**Ti**	**V**	**Cr**	**Mn**	**Fe**	**O**
Spot 1	0.01	0.01	3.38	3.52	0.00	nd	nd	0.00	1.71	12.0
Spot 2	0.00	0.54	3.30	3.34	0.00	0.00	nd	0.01	1.23	12.0
Spot 3	0.00	1.42	3.09	3.05	0.03	0.00	nd	0.11	0.47	12.0

[a]*nd refers to elemental concentrations below the detection limits of LA-ICP-MS.*

in the color of demantoid garnet are generally caused by traces of chromium (Cr^{3+}), ferric iron (Fe^{3+}), Fe^{2+}-Ti^{4+} intervalence charge transfer, and Fe^{2+}-Fe^{3+} interactions (G. Giuliani et al., "Gem andradite garnet deposits demantoid variety," *InColor*, No. 36, Summer 2017, pp. 28–39).

Recently, GIA's Bangkok laboratory received a 4.47 ct yellowish green gemstone for identification. Standard gemological testing, including a refractive index over the limits of the refractometer and a specific gravity of 3.86, and Raman spectroscopy identified it as demantoid garnet. Microscopic examination revealed strong internal graining, fingerprints, and particles mixed with short needles. Interestingly, it also exhibited transparent octahedral crystals at the crown (figure 6). Some of them reached the surface and had a different luster from the host material. Close examination showed that the crystals contained two different luster areas, which also distinguished them from the host demantoid (figures 7 and 8).

Raman spectroscopy was performed on the three different areas to identify the materials. The Raman spectra of the two areas of the crystals were similar to that of the host, matching with andradite garnet. Garnet species typically possess similar physical properties and crystal forms, but differ in chemical composition. For example, andradite is a calcium-iron garnet with the formula $Ca_3Fe_2(SiO_4)_3$, whereas grossular is a calcium-aluminum garnet with the formula $Ca_3Al_2(SiO_4)_3$. Those two garnet species are in the same isomorphous series and therefore have the same general chemical formula, but differ only in containing Fe or Al. Due to their similar Raman spectra, chemical analysis is better suited to separate the species of garnet.

In this case, laser ablation–inductively coupled plasma–mass spectrometry (LA-ICP-MS) was used to compare the chemical composition of the demantoid against that of the surface-reaching inclusions. Spot 1 was on the host material, spot 2 on the outer area of the crystal inclusion, and spot 3 on the inner area of the crystal (figure 8).

Surprisingly, the three spot areas exhibited different chemical compositions, especially between the host demantoid area and the inner area of

Figure 6. A cluster of transparent octahedral crystals observed in a yellowish green demantoid garnet. Field of view 1.2 mm.

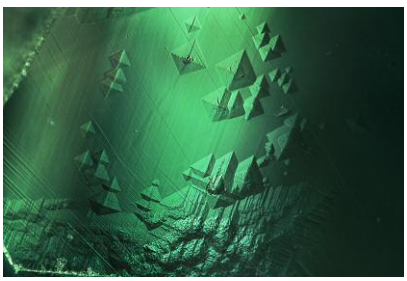

Figure 7. Some of the transparent octahedral crystals reached the surface of the demantoid. Field of view 2.0 mm.

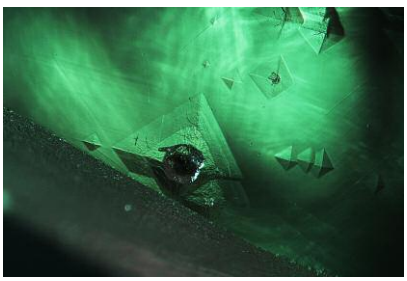

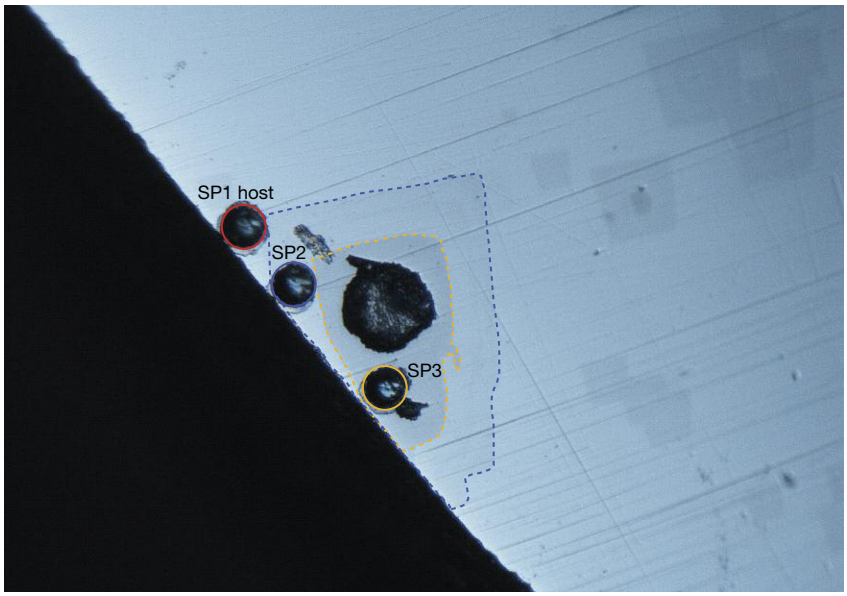

Figure 8. LA-ICP-MS was performed on three different areas: the host demantoid (spot 1), the outer area of the included crystal (spot 2), and the inner area of the included crystal (spot 3). The blue dashed line shows the separation between the demantoid area and the outer area of the inclusion. The yellow dashed line separates the outer and inner areas of the inclusion. Field of view 1.0 mm.

the crystal. This indicated that the crystal inclusion was from a garnet species other than andradite. Table 1 shows the chemical composition of the three spot areas, provided first in parts per million by weight (ppmw) units, followed by wt.% oxides of elements, and then as recalculated cations normalized to 12 oxygen atoms. Spot 1 (the demantoid) contained significantly more Fe than Al, whereas spots 2 and 3 of the crystal inclusion contained both elements. Spot 2 contained a higher concentration of Fe than Al, and the calculation showed a mix of two garnet species. It is possible that the detection area partly included the host material. Spot 3 contained a higher Al concentration than Fe (a 75.36% match with grossular).

Many types of solid inclusions are found in demantoid garnet, such as chromite, apatite, and diopside. From the results obtained here, it is interesting that solid inclusions of a different garnet species—grossular, in this case—can also be trapped in demantoid.

Ungkhana Atikarnsakul

Resin IMITATION IVORY with a Pseudo "Engine-Turned" Structure

Resin materials marketed as imitation ivory were recently acquired by a GIA gemologist. Material A, marketed under the name "Arvorin Plus," was purchased from a billiard store. Material B, sold as "Resin-Ivory+S," was purchased from a guitar store. These are manufactured as rods that can be purchased in a variety of lengths. Both show fine parallel linear striations along their length and a distinct pattern reminiscent of Schreger lines, commonly referred to as an "engine-turned" effect, when viewed across their horizontal plane (figure 9). These are also characteristics seen in genuine elephant and mammoth ivory.

The resin materials were found to have nearly identical gemological properties. Both had a Mohs hardness around 2, indented when pressed firmly with a pointer probe, and melted rapidly when touched with a hot point. They also had a spot refractive index reading of 1.57, a hydrostatic specific gravity of 1.24, and were inert to long-wave and short-wave ultraviolet light. Raman spectroscopy further confirmed their identity as a polymer substance.

Genuine elephant and mammoth ivory typically show a refractive index

Figure 9. Left: Material A, 24.40 mm in diameter and sold under the name "Arvorin Plus," shows parallel linear striations along its length and unorganized perpendicular striations along the horizontal plane. Right: Material B, 18.93 mm in diameter and marketed as "Resin-Ivory+S," exhibits parallel linear striations along its length and perpendicular striations with an average angle of 90° along its horizontal plane.

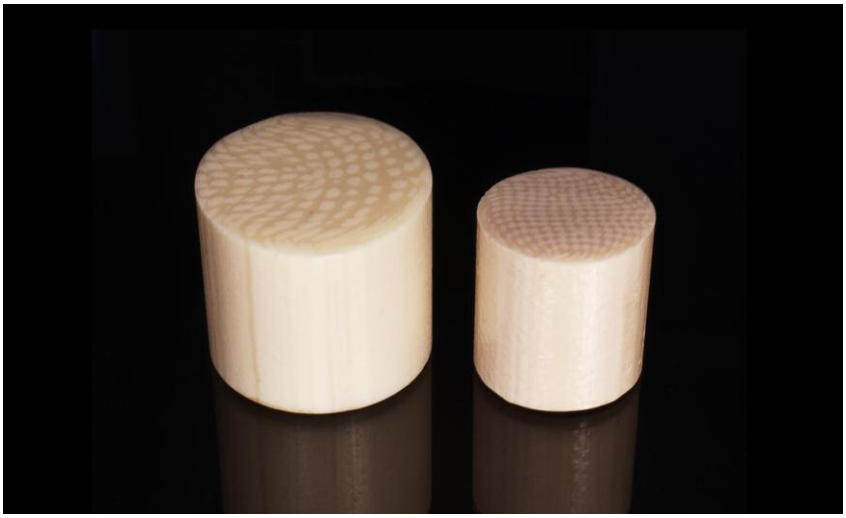

Figure 10. Left: Elephant ivory with Schreger lines intersecting at an average angle of 109°; field of view 19.27 mm. GIA Collection no. 4287. Right: Mammoth ivory with Schreger lines intersecting at an average angle of 69°; field of view 19.27 mm. Part of GIA Collection no. 19267, donated in 1995 by Richard Marcus of Mammoth Enterprises, Inc.

of 1.540, a specific gravity between 1.70 and 2.00, and weak white to blue fluorescence under both long-wave and short-wave UV. Ivory's most distinguishing characteristic is a display of Schreger lines ("engine turning"), an inherent growth property that is visible when specimens are cut perpendicular to the length of the tusk. These Schreger lines create unique angles that distinguish between mammoth and elephant species. When concave angles that open to the inner area of the tusk are measured, mammoth ivory will show an average angle of less than 90°, while elephant ivory will show an average angle greater than 90°. Figure 10 shows elephant and mammoth specimens oriented with their concave angles opening to the inner area of the tusk. Their Schreger lines intersect at average angles of 109° and 69°, respectively. These can be compared to materials A and B. While material A did show perpendicular striations along the horizontal plane, the angles were not particularly organized or consistently measurable. However, material B had "engine-turned" striations at an average angle of 90° along this same plane.

Cabochons were cut from both types of resin, and the form of a small elephant tusk was carved out of material A (figure 11). The resins' low hardness allowed them to be quickly ground down for shaping, while their high toughness prevented any chipping or fracturing even on small details. The resins each consist of two components with slightly different hardness, which produces the engine-turned pattern. One difficulty is that when attempting to shape a smooth surface, the darker and lighter areas erode at different speeds, creating an uneven texture. This effect is minimized, though, at the prepolishing stage of the carving. The low melting point of the ivory imitations posed an added challenge during the polishing process. When attempting to polish with a compound applied to a felt

Figure 11. Three ivory imitations carved for this study. The tusk (52.23 ct) and the cabochon on the right (35.37 ct) were created from material A. The cabochon on the left (14.67 ct) was created from material B. Lapidary by Dylan Hand.

wheel, the resins can melt and deform relatively quickly.

Elephant ivory was first regulated under the Endangered Species Act in 1976, with more recent laws creating a near-total ban on its import and export. Laws regarding mammoth ivory vary by state. Ivory imitations are now commonly used in their place for furniture and musical instrument inlays, jewelry, and various accessories. Both resins are purportedly composed of spun polyester and are being produced in China.

Britni LeCroy and Dylan Hand

Cobalt-Coated SAPPHIRE

Recently, the New York laboratory received a bright blue stone for identification. The blue color closely resembled that of the highly desired cobalt spinel. Advanced testing procedures of Fourier-transform infrared (FTIR), ultraviolet/visible/near-infrared (UV-Vis-NIR), energy-dispersive X-ray fluorescence (EDXRF), and laser Raman spectroscopy were performed to aid in identification. FTIR revealed a corundum spectrum, but with an uncharacteristic rise in the 7000–5800 cm^{-1} region. Laser Raman spectroscopy confirmed corundum, and UV-Vis-NIR yielded a cobalt absorption spectrum similar to that of diffused cobalt spinel.

Magnification revealed the presence of a coating, which was responsible for the observed over-the-limits RI reading. The coating was easily detected by the speckled, uneven surface and lighter facet edges where the coating was damaged (figure 12). EDXRF identified the coating as cobalt, consistent with the UV-Vis-NIR absorption spectrum. The stone possessed typical heated sapphire inclusions, such as altered fingerprints and frosted crystals. In addition, Raman spectroscopy identified glass-filled surface-reaching cavities (figure 13).

Cobalt coating is already a known treatment of tanzanite to improve the blue color component, but GIA has not observed cobalt coating on sapphire in recent years (see Spring 1994 *G&G*, pp. 48–49). Unlike cobalt coating on tanzanite, which has been observed applied only to the pavilion, this coating covered the entirety of the sapphire. This highlights the possibility of cobalt coating on materials other than tanzanite to induce a more pronounced blue color.

Figure 12. Lighter facet junctions and a speckled surface are evidence of coating. Field of view 4.79 mm.

Because of its color, this material is most likely to be mistaken for cobalt spinel, which can easily be eliminated as a possibility through standard gemological testing with the polariscope and specific gravity. The stone tested was doubly refractive and had a specific gravity of 4.00, while spinel is singly refractive and has an SG of 3.60 (+0.10/–0.03). Although the RI was over the limit of

Figure 13. Glass-filled cavities on the sapphire's pavilion. Field of view 3.57 mm.

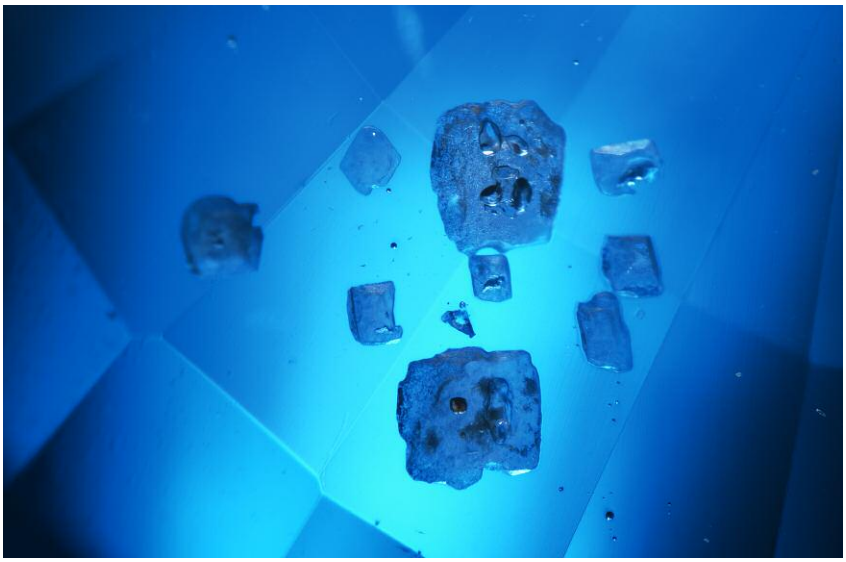

the refractive index liquid, the stone's specific gravity and doubly refractive nature point to sapphire. Advanced testing was useful in confirming the true identity of the stone and the coating.

Virginia Schneider and Jessica Jasso

Possible Natural Abalone SHELL Blister

An intriguing item was sent by KC Bell to GIA's Carlsbad laboratory for examination. Mr. Bell stated that it was found among a group of natural abalone pearls off the coast of Southern California in the Pacific Ocean. The sample (figure 14) weighed 3.00 ct, measured 10.73 × 8.82 × 6.23 mm, and was appealing because "pearl" layers appeared to have formed around a piece of rock. However, its natural or cultured origin and the mollusk species that produced it needed to be determined.

The sample consisted of two main components: an opaque dark body and a translucent cap formed of nacreous layers. The main body looked like a stone with a typical angular baroque shape expected of unfashioned natural material. The exposed areas exhibited a bumpy surface texture, and a strong fiber-optic light revealed a dark greenish bodycolor and some black areas of a different composition. Subsequently, Raman spectroscopic analysis with an 830 nm diode laser verified the dark greenish body was composed of a rock-forming feldspar mineral when the spectrum was matched with the RRUFF mineral database (RRUFF-R040129).

The thin layers partially covering the stone displayed vibrant blue, green, and purple-pink hues. At higher magnifications, a fine platelet structure was clearly visible, together with a characteristic underlying botryoidal-like structure that has been observed through the translucent surface layers of many abalone pearls (Fall 2015 Lab Notes, pp. 319–320). Raman analysis of the surface layers using a 514 nm argon-ion laser revealed peaks at 701, 705, and 1085 cm^{-1}, proving the nacre was composed of aragonite. In pearl testing, the higher excitation power of this laser is generally used in the identification of calcium carbonate polymorphs as well as natural pigments or artificial coloring agents. The 830 nm laser is used to obtain spectra in some situations, such as when high fluorescence is encountered with the 514 nm laser.

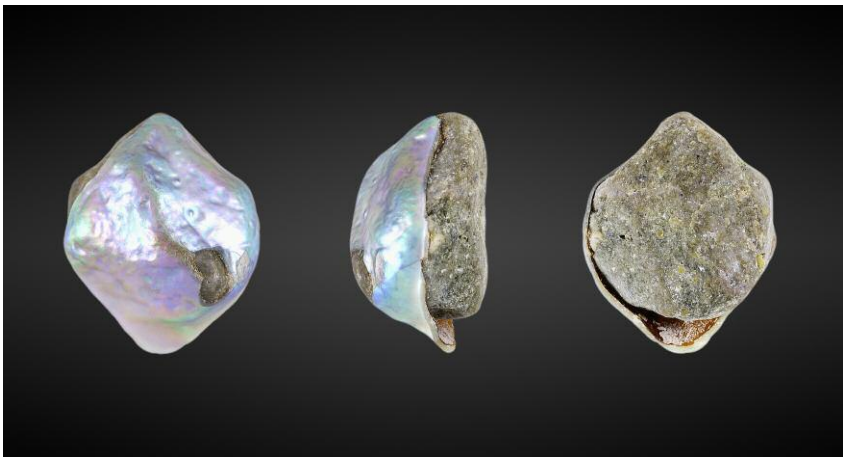

Figure 14. This intriguing abalone sample, shown in three different orientations, weighed 3.00 ct and measured 10.73 × 8.82 × 6.23 mm.

Energy-dispersive X-ray fluorescence (EDXRF) analysis showed that the nacreous surface layers contained low levels of manganese and confirmed a saltwater origin. Moreover, 221 ppm of iodine was detected, typical of many abalone shells and pearls since abalone is an iodine-rich organism (H.S. Doh and H.J. Park, "Speciation of bio-available iodine in abalone (*Haliotis discus hannai*) by high-performance liquid chromatography hyphenated with inductively coupled plasma-mass spectrometry using an *in vitro* method," *Journal of Food Science*, Vol. 83, No. 6, 2018, pp. 1579–1587). GIA has often detected iodine in abalone samples examined (Fall 2015 Lab Notes, pp. 319–320). Surface observation and chemical data confirmed that the nacre layers were produced by a univalve abalone gastropod (*Haliotis* genus), allowing us to confidently identify the mollusk species. Furthermore, EDXRF analysis of the rock surface revealed that it was composed of sodium-rich feldspar.

Closer examination of a small surface opening on the face of the sample (figure 15) and the edge of the nacre where it did not cover the underlying rock (figure 14, center and right) revealed a tight connection between the two main components. No gas bubbles or other features such as flow lines indicating an artificial bonding agent were observed in the translucent brown layer between them. The brown layer appeared to be an organic substance—likely conchiolin, an essential natural substance secreted by mollusks during the formation of pearls, blisters, and shells. The inter-

Figure 15. The overlying nacre tightly conformed to the underlying rock's surface, and a small opening was visible on the face, exposing the material beneath. A translucent brown layer between the two main components is possibly an organic substance, likely conchiolin. Field of view 7.19 mm.

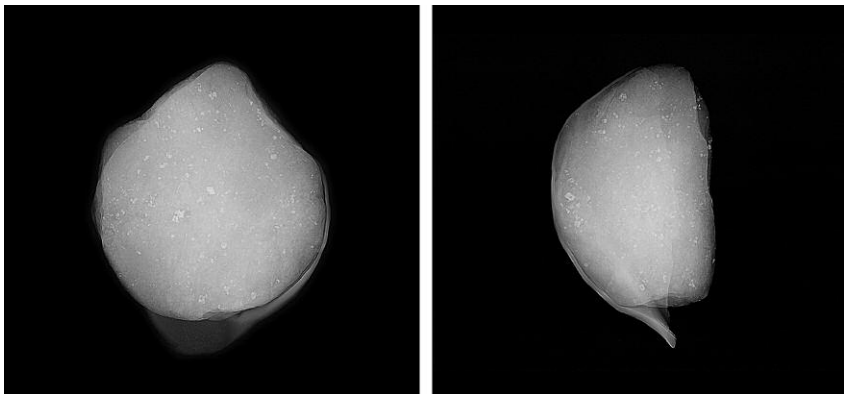

Figure 16. RTX images of the sample's face (left) and side (right) revealed that the thin nacre layer conformed very well to the underlying stone's surface.

nal structure revealed by real-time X-ray microradiography (RTX) supported the observational findings that the thin nacreous overgrowth adhered to the rock's surface in all directions and did not appear to have formed from any culturing process (figure 16).

Abalone are known to produce natural pearls and are also used commercially to produce cultured shell blisters in order to fashion assembled cultured blister "pearls" (mabe). Shell blisters can form naturally when a foreign object accidentally enters the mollusk's body and becomes trapped in between the shell's interior surface and the mantle tissue. If the mollusk survives this experience, the cells within the mantle tissue continue to secrete nacre (commonly biogenic aragonite) to increase the layers and cover the intruder, possibly to ease any discomfort. The intruder eventually becomes a part of the inner shell, resulting in a natural shell blister. Based on this formation mechanism and the gemological evidence obtained, this sample appears to be an unusual natural shell blister in which a small piece of rock acted as the irritant that initiated formation. Since abalone mollusks inhabit rocky areas and attach themselves to rocky surfaces, this scenario is not out of the question.

Artitaya Homkrajae

Large LABORATORY-GROWN STAR RUBY and SAPPHIRE

The Tokyo lab received for a Quality Assurance report two unusually large loose stones with asterism. One was a 4,759 ct red sphere (figure 17, left) with a diameter of approximately 76.96 mm, and the other a 467.2 ct blue cabochon measuring approximately 52.04 × 42.29 × 20.89 mm (figure 17, right).

These stones both had a spot refractive index of 1.77 and were doubly refractive with a uniaxial interference figure. The red sphere displayed a ruby spectrum with a handheld spectroscope. Microscopic observation showed curved bands of gas bubbles, cottony structure on the surface, and Plato striations (figure 18), providing proof of a laboratory-grown star ruby. The cottony structure indicates the possibility of diffusion treatment. The blue cabochon displayed a faint blue sapphire spectrum with the handheld spectroscope. It had a mottled blue color in diffused light (figure 19). Apparently it was a titanium-diffused colorless synthetic sapphire polished to produce asterism. As a result of polishing, the blue color is concentrated on the flat bottom and mottled on the curved top. This is visible when viewed from the side. Microscopic observation showed curved bands of gas bubbles, proof of laboratory growth.

As Schmetzer et al. summarized ("Dual-color double stars in ruby, sap-

Figure 17. A 4,759 ct synthetic star ruby and a 467.2 ct synthetic star sapphire were submitted to GIA's Tokyo lab.

Figure 18. Asterism seen on the surface and irregular grain boundaries (Plato striations). Field of view 11.4 mm.

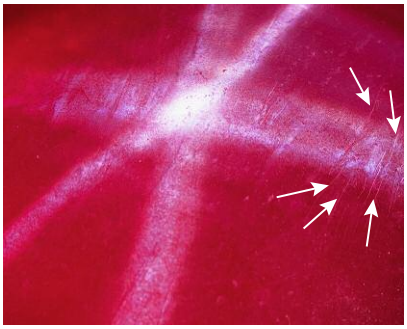

Figure 19. Mottled blue patterns were observed in the synthetic sapphire against transmitted illumination through a diffuser plate.

phire, and quartz: Cause and historical account," Summer 2015 *G&G*, pp. 112–143), the Czochralski pulling technique can produce large crystals. These crystals have a uniform distribution of color and titanium-bearing precipitates compared to other growth methods, and they can be cut from any part of the crystal, regardless of size. Therefore, this laboratory-grown star ruby was most likely produced by the pulling technique. Also, this specimen was too large to have been produced by flame fusion. Detailed information on these two items is not available, but they are probably similar products.

Synthetic star corundum is not rare, but these were among the largest laboratory-grown star rubies and star sapphires submitted to the GIA laboratory.

Masumi Saito and Yusuke Katsurada

LABORATORY-GROWN SAPPHIRE with Unusual Features

The Hong Kong laboratory recently examined a 14.36 ct pink-orange cushion mixed-cut specimen measuring 12.97 × 11.41 × 10.59 mm. Standard gemological testing yielded an RI of 1.760–1.768, a chromium emission line in red using a handheld spectroscope, strong red fluorescence under long-wave UV, and weak red fluorescence under short-wave UV. These properties were consistent with pink sapphire. Magnification revealed large fractures containing orange staining and some partially crystallized foreign material (figure 20). The foreign material partially crystallized in a dendritic pattern resembling that of diaspore (figure 21). Other natural-looking features included a twinning plane and tubules. Nonetheless, the observation of indistinct Plato lines and a slight curvature in the twinning plane raised suspicion about the stone's nature.

Figure 20. This 14.36 ct pink-orange synthetic sapphire contains large fractures with orange staining and some partially crystallized foreign material. Field of view 15.26 mm.

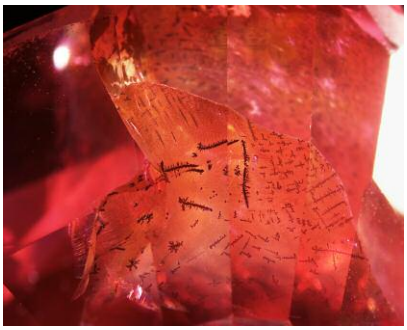

Figure 21. The foreign material partially crystallized in a dendritic pattern in the fractures, reminiscent of diaspore. Field of view 7.64 mm.

A strong red curved band observed in the DiamondView confirmed it was a Verneuil (flame-fusion) synthetic sapphire (figure 22). The absence of Ga, V, and Fe in the specimen, determined using laser ablation–inductively coupled plasma–mass spectrometry (LA-ICP-MS), provided further evidence supporting its synthetic nature. Ti was below detection limit in all six spots. Cr was below the detection limit in one spot and 37.61–44.31 ppma in five other spots.

Although flame-fusion synthetic sapphires are common in the marketplace, it is unusual to encounter a specimen containing such natural-looking orange staining and partially crystallized foreign material in the fractures. Careful observation as well as advanced testing are required for the correct identification of the natural or synthetic origin of such specimens.

Bona Hiu Yan Chow and Mei Mei Sit

VLASOVITE

The Carlsbad laboratory recently received for identification service a stone with properties that were not consistent with stones previously identified at GIA. This yellow octag-

Figure 22. The pink-orange specimen showed a strong red curved band in the DiamondView, confirming its identity as a flame-fusion synthetic sapphire.

Figure 23. This 1.20 ct octagonal modified brilliant was identified as the rare gem vlasovite.

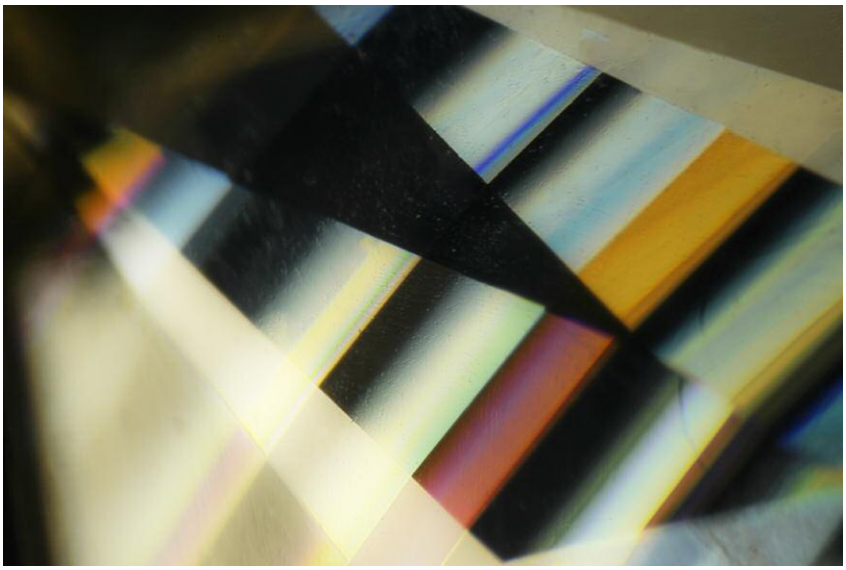

Figure 24. Colorful twinning planes were observed in the faceted vlasovite using polarized light. Field of view 3.23 mm.

onal modified brilliant (figure 23), measuring 6.41 × 5.26 × 4.68 mm, weighed 1.20 ct and had a specific gravity of 3.01. Microscopic features observed included distinct parallel twinning planes (figure 24), iridescent fractures, stringers, and fingerprints. Standard gemological testing revealed that it was doubly refractive, with a biaxial optic figure and a refractive index of 1.608–1.628. It fluoresced a very weak yellow under short-wave UV and had no reaction under long-wave UV. The Raman spectrum of the stone (figure 25) was matched to one in the RRUFF database, which confirmed the gem's identity as vlasovite, an inosilicate mineral with the chemical formula $Na_2ZrSiO_4O_{11}$ (rruff.info/vlasovite/R060913).

Vlasovite is known to be found in pegmatites in northern Russia, Canada, and Portugal. It was named after Kuzma Alekseevich Vlasov, who studied the region where vlasovite originated (handbookofmineralogy.com). Vlasovite is a rare mineral, and faceted stones are especially rare. This is the first faceted example examined at GIA's Carlsbad laboratory.

Jessa Rizzo

Figure 25. Raman spectroscopy confirmed the gem's identity as vlasovite.

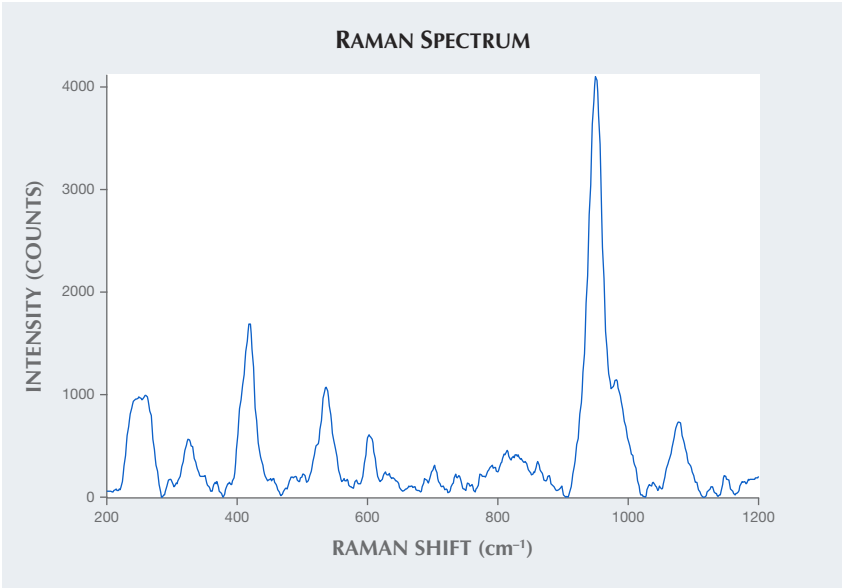

PHOTO CREDITS
Diego Sanchez—1, 3, 14, 23; Nathan Renfro—4; Maryam Mastery Salimi—5; Ungkhana Atikarnsakul—6, 7, 8; Dylan Hand—9, 10, 11; Britni LeCroy—10; Tyler Smith—12, 13; Artitaya Homkrajae—15; Shunsuke Nagai—17, 19; Masumi Saito—18; Moqing Lin—20, 21, 22; Jessa Rizzo—24